File S1: Supporting Information

1. Mutation matrix Q

Let C_n denote a random variable modeling a single base in generation n at some locus with state space the sequence alphabet $\mathcal{A}$. Let $c, d \in \mathcal{A}, c \neq d$, be two bases from the alphabet. The mutation rate per replication cycle is defined as the probability of not reproducing the same base

$$\mu := P\left(C_{n+1} \neq c \mid C_n = c\right) \tag{1.1}$$

As the mutation rate is assumed to be uniform for all bases, a transition from a single base to a specific other base has probability

$$P\left(C_{n+1} = d \mid C_n = c\right) = \frac{\mu}{|\mathcal{A}|-1} \tag{1.2}$$

The self-replication probability is

$$P\left(C_{n+1} = c \mid C_n = c\right) = 1-\mu \tag{1.3}$$

In order to set up the probabilities of mutation between haplotypes, we assume an independent and identical mutation rates across loci. Let $i, j \in \{1, \ldots, m\}, m = |\mathcal{A}|^L$, then we set for the mutation matrix $\mathbf{Q} = \left(q_{ij}\right)$

$$q_{ij} = \left(\frac{\mu}{|\mathcal{A}|-1}\right)^{d(i,j)} \cdot (1-\mu)^{L-d(i,j)} > 0 \tag{1.4}$$

where $d(i, j)$ denotes the Hamming distance, i.e., the number of loci at which haplotypes i and j differ. Since $q_{ij} = q_{ji}$, the matrix $\mathbf{Q}$ is symmetric.

A. Non-uniform transition/transversion rate

In order to account for a non-uniform mutation rate between different bases, the mutation model from (1.4) needs to be generalized. A mutation is called a *transition* when A $\leftrightarrow$ G or C $\leftrightarrow$ T during a replication cycle. The remaining mutations are called *transversions*, i.e., all mutations from a purine to a pyrimidine. With α we denote the probability of a transition, in line with the similar transition substitution parameter used in phylogenetic analysis. The probability of a transversion mutation occurring is denoted with β. The ratio of α/β is the transition/transversion ratio and is denoted by κ. These two mutation types can be combined to yield the overall mutation rate compatible with the definition in (1.1):

$$\mu = \alpha + 2\beta \tag{1.5}$$

The intuition of this identity is that, for every base, there exists exactly one transition mutation and two transversion mutations. The two mutation rates can now be expressed in terms of μ and κ as

$$\alpha = \mu \cdot \frac{\kappa}{\kappa+2}, \qquad \beta = \mu \cdot \frac{1}{\kappa+2} \tag{1.6}$$

For $\kappa = 1$, we find the specialization (1.2). To set up the mutation matrix for the full DNA sequence space $\mathcal{A}^L$, we use

$$q_{ij} = \alpha^{n_{\text{ti}}(i,j)} \cdot \beta^{n_{\text{tv}}(i,j)} \cdot (1-\mu)^{L-d(i,j)} \tag{1.7}$$

where $n_{\text{ti}}(i, j)$ respectively $n_{\text{tv}}(i, j)$ denote the number of transitions respectively transversions going from haplotype i to j and $d(i, j) = n_{\text{ti}}(i, j) + n_{\text{tv}}(i, j)$. It should be emphasized that, while α, β and κ bear resemblance to the parameters of the popular Kimura-2-Parameter model (also known as K80 model), the parameters used in constructing phylogenetic trees and the mutation rates here cannot be used interchangeably. Substitution parameters implicitly account for more effects, such as fixation and codon position effects, and cannot be equated with mutation rates (Kimura, 1980).

2. The function g

We ask for the equilibrium distribution $\mathbf{p} \in \Delta^{n-1}$ in the quasispecies model given a fitness landscape $\mathbf{f} \in \mathcal{F}^{n-1}$. The asterisk has been dropped from the distribution vector in (3) of the main article, as all further analysis will only be concerned with the equilibrium value of $\mathbf{p}(t)$. By (3) in the main article, for $\phi = 1$, the equilibrium distribution is

$$\mathbf{p} = \mathbf{Q}^T \operatorname{diag}(\mathbf{f})\,\mathbf{p} \tag{2.1}$$

The equilibrium distribution $\mathbf{p}$ lies in the kernel of the matrix

$$\mathbf{B} := \mathbf{Q}^T \operatorname{diag}(\mathbf{f}) - \mathbb{I}_n \tag{2.2}$$

where $\mathbb{I}_n$ denotes the $n \times n$ identity matrix. Employing the Moore-Penrose pseudoinverse (Searle, 1982), any vector in the kernel of $\mathbf{B}$ can be expressed as

$$\mathbf{a}(\mathbf{f}) := \left(\mathbb{I}_n - \mathbf{B}^+\mathbf{B}\right)\mathbb{1}_n \tag{2.3}$$

where $\mathbf{B}^+$ is the Moore-Penrose pseudoinverse of $\mathbf{B}$ and $\mathbb{1}_n$ denotes the n-dimensional vector of all-ones. We define the scalar normalization constant $\lambda(\mathbf{f}) := \mathbb{1}_n^T \mathbf{a}(\mathbf{f})$ and set

$$g(\mathbf{f}) := \frac{\mathbf{a}(\mathbf{f})}{\lambda(\mathbf{f})} = \ker(\mathbf{B}) \cap \Delta^{n-1} \tag{2.4}$$

such that $g(\mathbf{f}) \in \Delta^{n-1}$. The function is well-defined, because $\left|\ker(\mathbf{B}) \cap \Delta^{n-1}\right| = 1$ for all $\mathbf{f} \in \mathcal{F}^{n-1}$ due to the Perron-Frobenius theorem (Bapat and Raghavan, 1997). It is not surjective, because the quasispecies equation has the property that no haplotypes can go extinct, as mutations of any haplotype will always produce all other haplotypes with non-zero probability. Thus, there exists a non-empty set of distributions, that include faces of Δ^{n-1}, which cannot arise in steady state from the quasispecies equation. We hence restrict g to its image $g : \mathcal{F}^{n-1} \to \operatorname{image}(g) =: \mathcal{Q}^{n-1} \subsetneq \Delta^{n-1}$, such that g is surjective. We refer to $\mathcal{Q}^{n-1}$ as the quasispecies space, i.e., the set of all equilibrium distributions the quasispecies equation can yield. In section B we have devised a two-haplotype model and derive lower and upper bounds on the relative frequencies defining $\mathcal{Q}^1$ that are directly related to the mutation rate of the polymerase.

A. The bijections g and h are inverses of each other

Theorem 1. *g is a bijection and h is its inverse.*

Proof. Given that g is surjective, all we have to show is

$$h(g(\mathbf{f})) = \mathbf{f} \quad \text{for all } \mathbf{f} \in \mathcal{F}^{n-1} \tag{2.5}$$

For proving (2.5), the following expansion is permissible, as $\mathbf{a}(\mathbf{f})$ is strictly positive due to the Perron-Frobenius theorem

$$\mathbf{f} = \operatorname{diag}(\mathbf{a}(\mathbf{f}))^{-1} \operatorname{diag}(\mathbf{a}(\mathbf{f}))\,\mathbf{f} \tag{2.6}$$

$\mathbf{Q}^{-T}\mathbf{Q}^T = \mathbb{I}_n$ as $\mathbf{Q}$ is regular due to it being a strictly diagonal dominant matrix

$$= \operatorname{diag}(\mathbf{a}(\mathbf{f}))^{-1} \mathbf{Q}^{-T}\mathbf{Q}^T \operatorname{diag}(\mathbf{a}(\mathbf{f}))\,\mathbf{f} \tag{2.7}$$

$$= \operatorname{diag}(\mathbf{a}(\mathbf{f}))^{-1} \mathbf{Q}^{-T}\mathbf{Q}^T \operatorname{diag}(\mathbf{f})\,\mathbf{a}(\mathbf{f}) \tag{2.8}$$

$$= \operatorname{diag}(\mathbf{a}(\mathbf{f}))^{-1} \mathbf{Q}^{-T}\left(\mathbf{Q}^T \operatorname{diag}(\mathbf{f})\,\mathbf{a}(\mathbf{f}) - \mathbb{I}_n\mathbf{a}(\mathbf{f}) + \mathbf{a}(\mathbf{f})\right) \tag{2.9}$$

$$= \operatorname{diag}(\mathbf{a}(\mathbf{f}))^{-1} \mathbf{Q}^{-T}\left(\mathbf{B}\mathbf{a}(\mathbf{f}) + \mathbf{a}(\mathbf{f})\right) \tag{2.10}$$

$$= \operatorname{diag}(\mathbf{a}(\mathbf{f}))^{-1} \mathbf{Q}^{-T}\left(\mathbf{B}\left(\mathbb{I}_n - \mathbf{B}^+\mathbf{B}\right)\mathbb{1}_n + \mathbf{a}(\mathbf{f})\right) \tag{2.11}$$

$$= \operatorname{diag}(\mathbf{a}(\mathbf{f}))^{-1} \mathbf{Q}^{-T}\left(\left(\mathbf{B} - \mathbf{B}\mathbf{B}^+\mathbf{B}\right)\mathbb{1}_n + \mathbf{a}(\mathbf{f})\right) \tag{2.12}$$

We have $\mathbf{B} - \mathbf{B}\mathbf{B}^+\mathbf{B} = 0$ by definition of the Moore-Penrose pseudoinverse, hence

$$\mathbf{f} = \operatorname{diag}(\mathbf{a}(\mathbf{f}))^{-1} \mathbf{Q}^{-T}\mathbf{a}(\mathbf{f}) \tag{2.13}$$

$$= \operatorname{diag}(\mathbf{a}(\mathbf{f}))^{-1} \mathbf{Q}^{-T}\mathbf{a}(\mathbf{f})\,\frac{\lambda(\mathbf{f})}{\lambda(\mathbf{f})} \tag{2.14}$$

$$= \operatorname{diag}\left(\frac{\mathbf{a}(\mathbf{f})}{\lambda(\mathbf{f})}\right)^{-1} \mathbf{Q}^{-T}\,\frac{\mathbf{a}(\mathbf{f})}{\lambda(\mathbf{f})} \tag{2.15}$$

$$= \operatorname{diag}(g(\mathbf{f}))^{-1} \mathbf{Q}^{-T} g(\mathbf{f}) \tag{2.16}$$

$$= h(g(\mathbf{f})) \tag{2.17}$$

□

B. Explicit description of $\mathcal{Q}^1$

Calculating the set $\mathcal{Q}^{n-1}$ is analytically not possible, but bounds can be formulated component-wise. Consider the two-haplotype model, where we find for the first component of $g(\mathbf{f})$, using MATLAB's symbolic toolbox,

$$p_1 = \frac{2f_2q_{21} - f_2 + 1}{f_1 - f_1q_{11} + f_2q_{21} - f_1f_2q_{11} + f_1f_2q_{21} + 1} \tag{2.18}$$

Since elements in $\mathcal{F}^{n-1}$ only have one degree of freedom when $n = 2$, we can replace f_2 with the help of the average fitness constraint $1 = p_1f_1 + p_2f_2$ and substitute into (2.18) to obtain

$$\left(\frac{1-p_1f_1}{1-p_1}\right)(2q_{21}-1)+1 = p_1\left(\left(\frac{1-p_1f_1}{1-p_1}\right)(q_{21}-f_1q_{11}+f_1q_{21})+f_1-f_1q_{11}+1\right) \tag{2.19}$$

In the limit as $f_1 \to 0$, this equation becomes

$$0 = p_1^2 + p_1(-q_{21}-2) + 2q_{21} \tag{2.20}$$

with roots $p_1 = q_{21}$ and $p_1 = 2$. Only the first yields a valid solution, namely $\mathbf{p} = (q_{21}, q_{22})^T$. The procedure can be repeated in an analogous fashion for $f_2 \to 0$ which then yields $\mathbf{p} = (q_{12}, q_{11})^T$. Thus, for the two-strains model, we have the component-wise bounds for $\mathbf{p} \in \mathcal{Q}^1$

$$q_{21} < p_1 < q_{11} \tag{2.21}$$
$$q_{12} < p_2 < q_{22} \tag{2.22}$$

3. Jacobian of h

In order to calculate the determinant of the Jacobian, the explicit form of the Jacobian needs to be known. Recall that

$$\operatorname{diag}(\mathbf{p})\,\mathbf{f} = \mathbf{p} \odot \mathbf{f} = \mathbf{f} \odot \mathbf{p} = \operatorname{diag}(\mathbf{f})\,\mathbf{p} \tag{3.1}$$

where $\odot$ denotes the Hadamard product (element-wise multiplication). To determine the Jacobian of

$$h(\mathbf{p}) = \operatorname{diag}(\mathbf{p})^{-1}\mathbf{Q}^{-T}\mathbf{p}, \tag{3.2}$$

we write

$$\mathbf{p} \odot h(\mathbf{p}) = \mathbf{Q}^{-T}\mathbf{p}, \tag{3.3}$$

and perform implicit differentiation,

$$\frac{\partial}{\partial \mathbf{p}}\left(\mathbf{p} \odot h(\mathbf{p})\right) = \frac{\partial}{\partial \mathbf{p}}\left(\mathbf{Q}^{-T}\mathbf{p}\right) \tag{3.4}$$

$$\operatorname{diag}(h(\mathbf{p}))\,\mathbb{I}_n + \operatorname{diag}(\mathbf{p})\,\frac{\partial h}{\partial \mathbf{p}} = \mathbf{Q}^{-T} \tag{3.5}$$

$$\frac{\partial h}{\partial \mathbf{p}} = \operatorname{diag}(\mathbf{p})^{-1}\,\mathbf{Q}^{-T} - \operatorname{diag}(\mathbf{p})^{-1}\operatorname{diag}(h(\mathbf{p})) \tag{3.6}$$

$$\frac{\partial h}{\partial \mathbf{p}} = \operatorname{diag}(\mathbf{p})^{-1}\,\mathbf{Q}^{-T} - \operatorname{diag}(\mathbf{p})^{-1}\operatorname{diag}\left(\operatorname{diag}(\mathbf{p})^{-1}\mathbf{Q}^{-T}\mathbf{p}\right) \tag{3.7}$$

The inner-most multiplication with $\operatorname{diag}(\mathbf{p})^{-1}$ in the last term of (3.7) can be factorized as it already is a diagonal matrix, hence

$$\mathbf{J} = \frac{\partial h}{\partial \mathbf{p}} = \operatorname{diag}(\mathbf{p})^{-1}\,\mathbf{Q}^{-T} - \operatorname{diag}(\mathbf{p})^{-2}\operatorname{diag}\left(\mathbf{Q}^{-T}\mathbf{p}\right) \tag{3.8}$$

4. Functional form of posterior density function

In order to devise an efficient inference scheme, we introduce the logistic transformation (Aitchison, 1982) $t : \mathbb{R}^{n-1} \to \Delta^{n-1}$,

$$t_i(\mathbf{y}) = \begin{cases} \dfrac{\exp(y_i)}{C(\mathbf{y})} & (i = 1, \ldots, n-1) \\ \dfrac{1}{C(\mathbf{y})} & (i = n) \end{cases} \qquad \mathbf{y} \in \mathbb{R}^{n-1} \tag{4.1}$$

where $C(\mathbf{y}) = 1 + \sum_{j=1}^{n-1} y_j$, and its inverse $t^{-1} : \Delta^{n-1} \to \mathbb{R}^{n-1}$,

$$t_i^{-1}(\mathbf{p}) = \log \frac{p_i}{p_n} \qquad (i = 1, \ldots, n-1) \qquad \mathbf{p} \in \Delta^{n-1} \tag{4.2}$$

The transformations t and t^{-1} are illustrated on the left side of Figure 1 in the main article.

We derive the functional form of the posterior density function on sample space $\mathbb{R}^{n-1}$, given data $\mathbf{X}$. This requires two transformations of the original probability density function, one from $\mathcal{F}^{n-1}$ to $\mathcal{Q}^{n-1}$ and then from $\mathcal{Q}^{n-1}$ to $\mathbb{R}^{n-1}$. For the first transformation,

$$p_{\mathcal{Q}}(\mathbf{p}) = |\det(\mathbf{J}[h](\mathbf{p}))| \cdot p_{\mathcal{F}}(h(\mathbf{p})) \tag{4.3}$$

where $p_{\mathcal{F}}(h(\mathbf{p})) = \text{const.}$ as we employ a uniform prior on $\mathcal{F}^{n-1}$

$$= |\det(\mathbf{J}[h](\mathbf{p}))| \cdot \text{const.} \tag{4.4}$$

where $p_{\mathcal{Q}}(\mathbf{p})$ denotes the transformed prior on $\mathcal{Q}^{n-1}$ and $\mathbf{J}[h](\mathbf{p}) = \dfrac{\partial h}{\partial \mathbf{p}}$ denotes the Jacobian of h with respect to $\mathbf{p}$ evaluated at some $\mathbf{p}$. We refer to section 3 for the derivation of the Jacobian

$$\mathbf{J}[h](\mathbf{p}) = \operatorname{diag}(\mathbf{p})^{-1}\mathbf{Q}^{-T} - \operatorname{diag}(\mathbf{p})^{-2}\operatorname{diag}\left(\mathbf{Q}^{-T}\mathbf{p}\right) \tag{4.5}$$

Second, we transform the previous prior on $\mathcal{Q}^{n-1}$ to $\mathbb{R}^{n-1}$. For conciseness, we calculate $\mathbf{p} = t(\mathbf{y})$ beforehand

$$p_{\mathbb{R}}(\mathbf{y}) = |\det(\mathbf{J}[t](\mathbf{y}))| \cdot p_{\mathcal{Q}}(\mathbf{p} = t(\mathbf{y})) \tag{4.6}$$

$$= \left(\prod_{i=1}^{n} t_i(\mathbf{y})\right) \cdot p_{\mathcal{Q}}(\mathbf{p} = t(\mathbf{y})) \tag{4.7}$$

Substituting for $p_{\mathcal{Q}}(\mathbf{p} = t(\mathbf{y}))$ with $|\det(\mathbf{J}[h](\mathbf{p} = t(\mathbf{y})))| \cdot \text{const.}$ from (4.4) gives

$$= \left(\prod_{i=1}^{n} p_i\right) \cdot |\det(\mathbf{J}[h](\mathbf{p} = t(\mathbf{y})))| \cdot \text{const.} \tag{4.8}$$

$$= \left|\det\left(\mathbf{Q}^{-T} - \operatorname{diag}(\mathbf{p})^{-1}\operatorname{diag}\left(\mathbf{Q}^{-T}\mathbf{p}\right)\right)\right| \cdot \text{const.} \tag{4.9}$$

$$= d(\mathbf{y}) \cdot \text{const.} \tag{4.10}$$

where we denote the absolute value of the determinant as $d(\mathbf{y}) := \left|\det\left(\mathbf{Q}^{-T} - \operatorname{diag}(\mathbf{p})^{-1}\operatorname{diag}\left(\mathbf{Q}^{-T}\mathbf{p}\right)\right)\right|$. Thus, the posterior has the functional form

$$p_{\mathbb{R}}(\mathbf{y} \mid \mathbf{X}) = \frac{P(\mathbf{X} \mid \mathbf{p}) \cdot d(\mathbf{y}) \cdot \text{const.}}{P(\mathbf{X})} \tag{4.11}$$

As the normalization constant $P(\mathbf{X})$ cannot be determined, we drop it and write for the posterior density function

$$p_{\mathbb{R}}(\mathbf{y} \mid \mathbf{X}) = P(\mathbf{X} \mid \mathbf{p}) \cdot d(\mathbf{y}) = d(\mathbf{y}) \cdot \left(\prod_{i=1}^{n} p_i^{X_i}\right) \cdot \text{const.} \tag{4.12}$$

For reasons of numerical stability, we use the logarithm

$$\log p_{\mathbb{R}}(\mathbf{y} \mid \mathbf{X}) = \log d(\mathbf{y}) + \sum_{i=1}^{n} X_i \log p_i + \text{const.} \tag{4.13}$$

5. Simulations

To highlight the numerical and parameter robustness of our model, we have conducted multiple simulations. For the sake of demonstration, unless stated otherwise, we have set $\kappa = 1$.

A. Numerical precision simulations

A crucial point for numerical stability lies in calculating the determinant in $d(\mathbf{y})$ in (4.13). As a sanity check, we ran the sampling procedure with a total of 0 reads for two haplotypes, which is equivalent to sampling from the prior. A correct sampling procedure will yield a flat distribution of the random variable $f_1 - f_2$, where f_1 is the fitness of haplotype 1 and f_2 is the fitness of haplotype 2. The results are depicted in Figure S1.

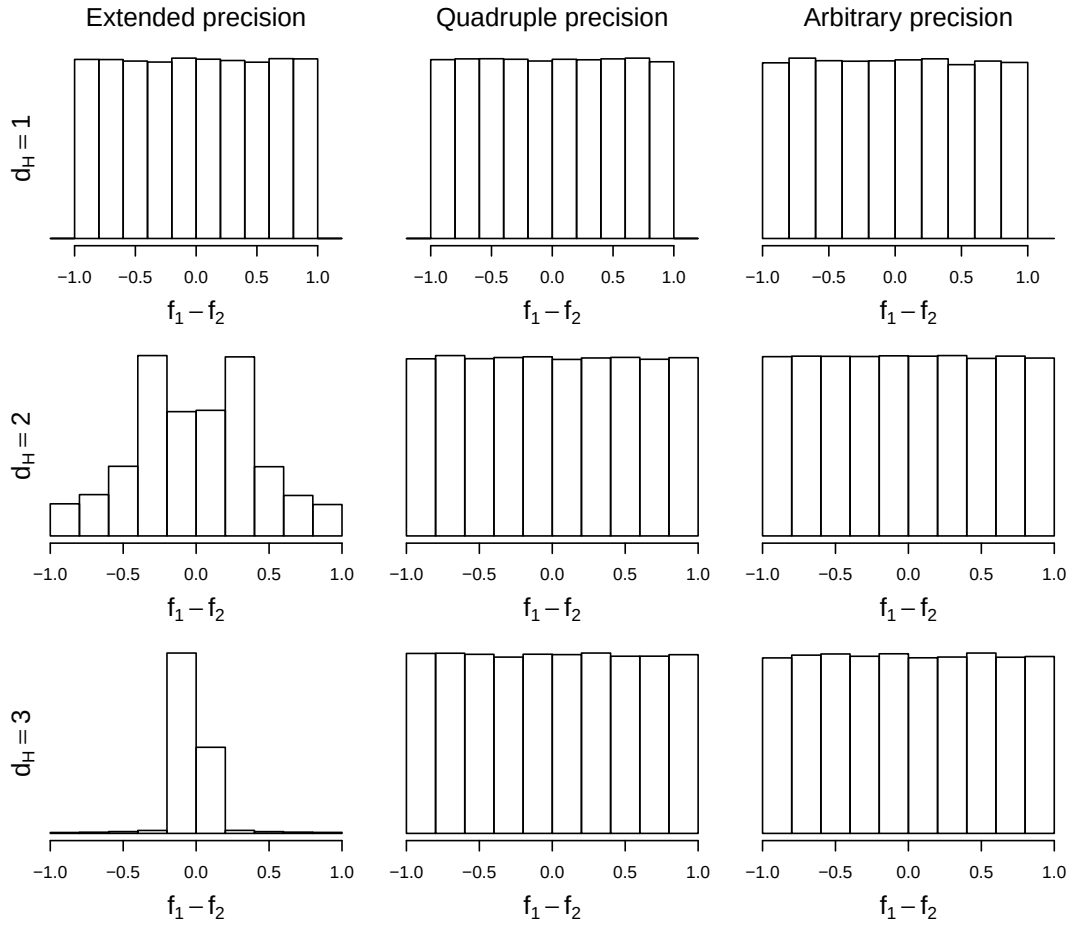

Figure S1. Prior fitness distributions for the two-haplotype model. Each column indicates a sampling procedure run with a specific precision and each row represents a haplotype constellation where haplotypes were separated by a different Hamming distance d_H.

For this simulation, the first haplotype was set to `AAA` and the second was set to `AAT`, `ATT`, and `TTT` for Hamming distances $d_H = 1$, 2, and 3, respectively. All constellations were run with $200 \cdot 10^6$ MCMC trials from the prior and a thinning interval of 1000, yielding 200 000 samples after each procedure.

The first column in Figure S1 depicts samples from the standard sampler, where floating point was performed with ordinary x87 floating point (about 18 digits of decimal precision). The second column depicts samples for 128-bit quadruple precision which was performed with GCC's `__float128` type (about 34 digits of decimal precision). The last column shows samples for running our sampling procedure with GMP's arbitrary precision type `mpf_t` (set to around 100 digits of decimal precision). Correct samplers should show a uniform distribution, as there is no fitness difference when sampling from the prior.

When the haplotype graph G_k is determined by $k = 2$, that is, the maximum number of mutations per step required for a haplotype to mutate into any other haplotype, then standard precision results cannot be trusted anymore. This is due to excessive floating-point rounding and absorption issues and motivates the requirement of $k < 2$ introduced in section *Haplotype space and mutation probabilities* of the main article. While we provide our sampler with the option of easily enabling quadruple and arbitrary precision floating point arithmetic, the performance penalties experienced by these types makes their use viable only for small haplotype sets $\mathcal{H}$.

B. Unobserved haplotypes simulations

In order to verify that the procedure detailed in the section *Haplotype space and mutation probabilities* of the main article allows for inference on data sets where the graph of observed haplotypes G_1 is not strongly connected, we conducted further simulations. We employed the same two observed haplotypes with the same varying d_H as in the previous section, that is, one observed haplotype is `AAA` and the second observed haplotype is `AAT`, `ATT` or `TTT` depending on d_H. In addition, we assumed that each haplotype was observed with exactly one read. From the symmetry of this setting and the observations, the differences of fitness values between the observed haplotypes should be symmetrical and not credibly different from 0. To circumvent the previously apparent numerical issues, we take the union of the haplotypes of the smaller d_H and the observed second haplotype for $\mathcal{H}$, such that the resulting G_1 is strongly connected. Due to the increased number of unobserved haplotypes in $\mathcal{H}$ now compared to the $\mathcal{H}$ in the previous section, the efficiency of the sampler is reduced, owing to an increased number of proposals not being an element of $\mathcal{Q}^{n-1}$. We run the sampling procedure with $100 \cdot 10^6$ MCMC trials and a thinning number of 100, the results of which are depicted in Figure S2.

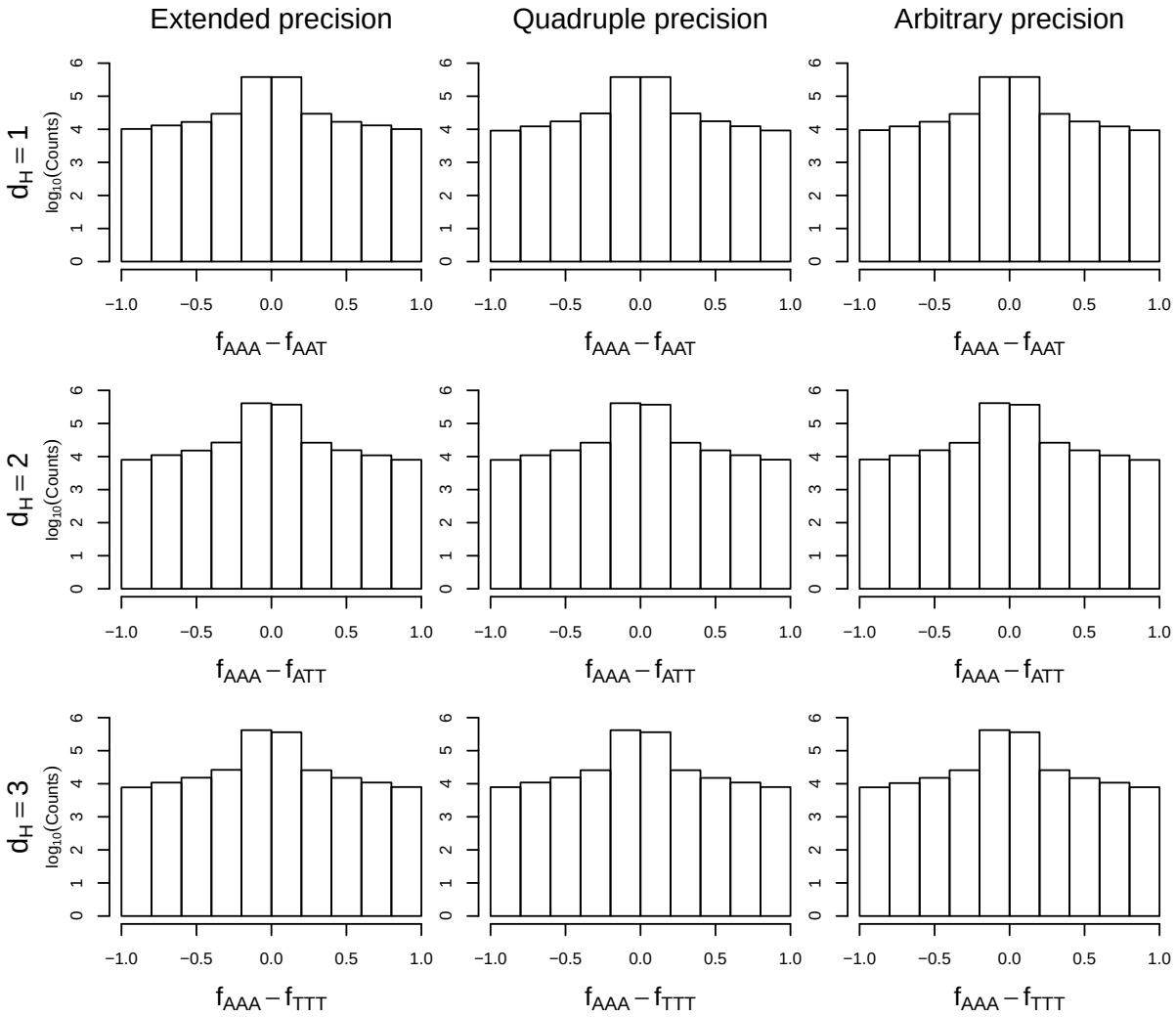

Figure S2. Posterior fitness difference distributions for the two-haplotype model with unobserved haplotypes. Each column indicates a sampling procedure run with a specific precision and each row represents a haplotype constellation where observed haplotypes were separated by a different Hamming distance d_H. As we are dealing with the posterior, the fitness differences are not uniformly distributed anymore. Due to the non-linear transformation involved in transforming probability distributions between different spaces, the tails of the posterior distribution of the fitness differences of the two observed haplotypes are heavy-tailed, hence the y-axis representing logarithmic counts.

To further assess the stability of the procedure of including unobserved haplotypes into $\mathcal{H}$, we tested whether for the same d_H, the posterior fitness samples depicted in Figure S2 come from the same distribution, i.e., whether there exists a difference between extended precision and the other numerical precision modes. To this end, we tested the difference with the Wilcoxon rank sum test, with results shown in Table S1.

As none of the differences in distributions between numerical precision modes is statistically significant at the 5% level, this demonstrates the numerical robustness of the method when including unobserved haplotypes. Lastly, as a sanity check, the 95% credibility intervals of Δf were determined for all precision modes (Table S2).

All of the credibility intervals include 0 as expected, providing a further indication that no spurious fitness differ-

Table S1. Testing for differences between precision modes for the last 50 000 samples of each run. Here $\Delta f_{\text{extended precision}}$ for instance denotes the random variable $f_{\texttt{AAA}} - f_{\texttt{AAT}}$ when $d_H = 1$ and extended precision was employed, i.e., the same samples as shown in Figure S2 in the top-left histogram.

$\mathbf{d_H}$	$\Delta f_{\text{extended precision}} - \Delta f_{\text{quadruple precision}}$	$\Delta f_{\text{extended precision}} - \Delta f_{\text{arbitrary precision}}$
	p-Value	**p-Value**
1	0.3606	0.2326
2	0.1603	0.4844
3	0.6719	0.7782

Table S2. Determining 95% credibility intervals for fitness differences. All intervals include 0, such that no difference in fitness between observed haplotypes can be called.

$\mathbf{d_H}$	$\Delta f_{\text{extended precision}}$	$\Delta f_{\text{quadruple precision}}$	$\Delta f_{\text{arbitrary precision}}$
1	$[-0.614, 0.625]$	$[-0.636, 0.547]$	$[-0.600, 0.596]$
2	$[-0.563, 0.537]$	$[-0.573, 0.506]$	$[-0.558, 0.507]$
3	$[-0.548, 0.524]$	$[-0.528, 0.545]$	$[-0.530, 0.551]$

ences are called due to numerical errors.

C. Upper bound on deviation from equilibrium

To give an upper bound on how close the viral population has to be to the equilibrium, we performed dynamical simulations on the quasispecies equation. To this end, we used the same LK parameters as in the section *LK fitness landscape simulations* of the main article. The random fitness landscapes were rescaled such that the average arithmetic sum of the fitness landscape is 1. This was done to bring the average generation time to approximately one unit of time. We randomly selected one haplotype as initial starting point and simulated the system up to 10^4 time units using MATLAB. We performed the same rank-based analysis as in the *simulation studies* section of the main article, namely studying the goodness of recovering the ranks of the fitness landscape, using (6) of the main article and the ranks of the frequency vector **p**. We analyzed the goodness of recovering the ranks as a function of stepping back in time, employing a total number of $N = 10\,000$ simulation points. Results for $L = 3$ are shown in Figure S3.

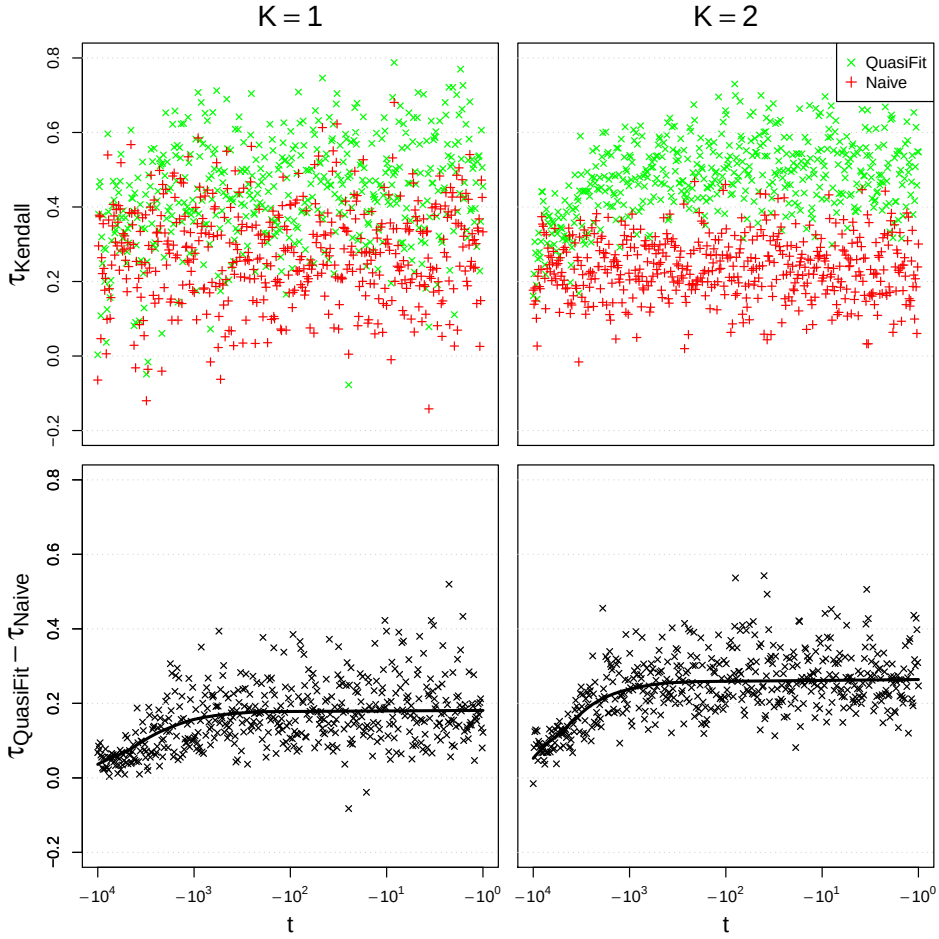

Figure S3. Accuracy of the predicted fitness landscape τ_{Kendall} as a function of the time t from equilibrium. We set $L = 3$ and analyzed the cases for $K = 1, 2$. The upper row shows the ability of the two methods to recover the fitness ranks. The bottom row illustrates the differences between the two methods. The thick solid line indicates the average distance between both methods as a function of time. For sake of clarity only 500 points are shown.

As can be seen, the *QuasiFit*-based estimator is clearly superior up to about 500 time units and degrades beyond. Nonetheless, even very far from equilibrium, the difference between both methods still marginally favors the *QuasiFit*-based estimator. Of these $N = 10\,000$ simulations, only 39 respectively 2 resulted in a better ranking of the true fitness landscape for the naive estimator for $K = 1$ respectively $K = 2$. As such, it can be concluded that the *QuasiFit*-based estimator is at least as good as the current standard of practice of taking the counts as estimator for the ranks of the fitness landscape, even when equilibrium has not been reached.

D. Deviations from transition/transversion ratio

To assess the violations of the assumed transition/transversion ratio, we conducted simulations by varying κ in (1.7). In detail, we increased κ from 1 (i.e., the uniform mutation model) up to 10 with $N = 10\,000$. For each simulation, we generated random LK fitness landscapes using the same parameters as in the previous section, calculated the quasispecies distribution using $1 < \kappa < 10$ and assumed the standard HIV mutation rate of $\mu = 3 \cdot 10^{-5}$. We then employed the standard uniform mutation matrix $\mathbf{Q}$ from (1.4) to simulate inference results for the standard *QuasiFit* case (Figure S4).

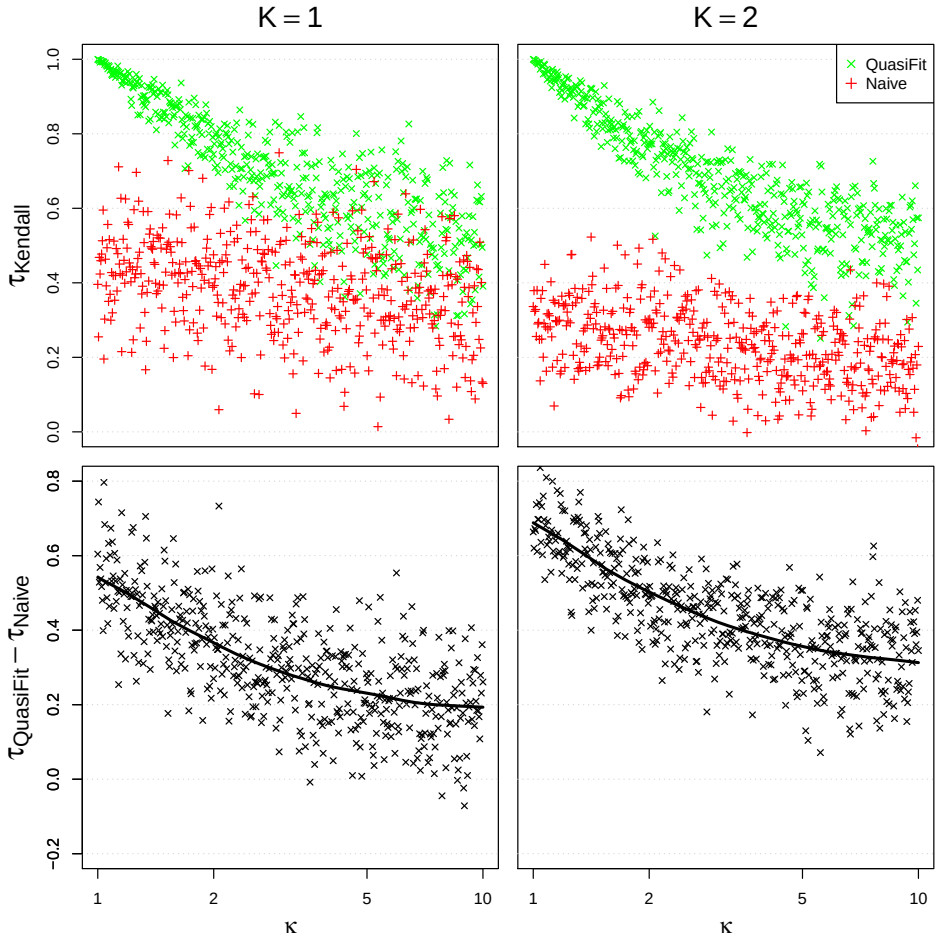

Figure S4. Accuracy of the predicted fitness landscape τ_{Kendall} as a function of the actual κ. We set $L = 3$ and analyzed the cases for $K = 1, 2$. The upper row shows the ability of the two methods to recover the fitness ranks. The bottom row illustrates the differences between the two methods. The thick solid line indicates the average distance between both methods as a function of the actual κ. For sake of clarity only 500 points are shown.

Our model is robust to at least some variation in κ. One study estimated κ to lie between 3.1 and 5.5 (Abram *et al.*, 2010). In this interval, the *QuasiFit* estimator is still better than calling fitness ranks by frequencies. In order to give the user a maximum of flexibility in inference, *QuasiFit* can also employ the mutation matrix from (1.7) to avoid possibly spurious results due to a misspecified model.

E. Epistastic vs. additive effects

In order to further understand how well the *QuasiFit* model can predict the ranks of a fitness landscape with varying levels of epistasis, we rewrite the fitness landscape as a full linear interaction model,

$$f(a_1,\ldots,a_L) = \sum_{i=1}^{L} \beta_{i,a_i} + \sum_{i=1}^{L-1}\sum_{j=i+1}^{L} \beta_{i,a_i;j,a_j} + \sum_{i=1}^{L-2}\sum_{j=i+1}^{L-1}\sum_{k=j+1}^{L} \beta_{i,a_i;j,a_j;k,a_k} + \ldots \tag{5.1}$$

where β_{i,a_i} denote the additive effects of base a at locus i, $\beta_{i,a_i;j,a_j}$ denote the pair-wise epistatic effects of base a at locus i and base b at locus j and so on. For the simulations we continued to employ the log-normal distribution as in section *LK fitness landscape simulations* of the main article. Additionally, we parametrized the log-normal distribution of the epistatic effects $\beta_{i,a_i;(\cdot)}$ such that $\text{median}\left(\beta_{i,a_i;(\cdot)}/\beta_{i,a_i}\right) = C$. Hence, the epistatic and additive effects are identically distributed when $C = 1$. We refer to C as the strength of epistasis relative to the additive effects. In order for the results of this interaction model to be comparable to the results of the LK simulations, for a given K, we only included effects up to order $K+1$, e.g., if we set $K = 1$ we only included pair-wise epistatic effects $\beta_{i,a;j,b}$ and set all higher-order effects to 0.

For the simulations, we proceeded in a similar fashion as in the previous section, instead for every random fitness landscape we now generated a multinomial sample with 100 000 reads possessing a fitness MLE. Generating samples possessing an $\hat{\mathbf{f}}$ was done solely to aid inference, as $\hat{\mathbf{f}}$ can then be used as a proxy for the full Bayesian estimator. In total we simulated $N = 10\,000$ fitness landscapes with C in the interval $[3\cdot 10^{-2}, 3]$. The results of the *QuasiFit* fitness rank estimator versus the naively estimated ranks are depicted in Figure S5.

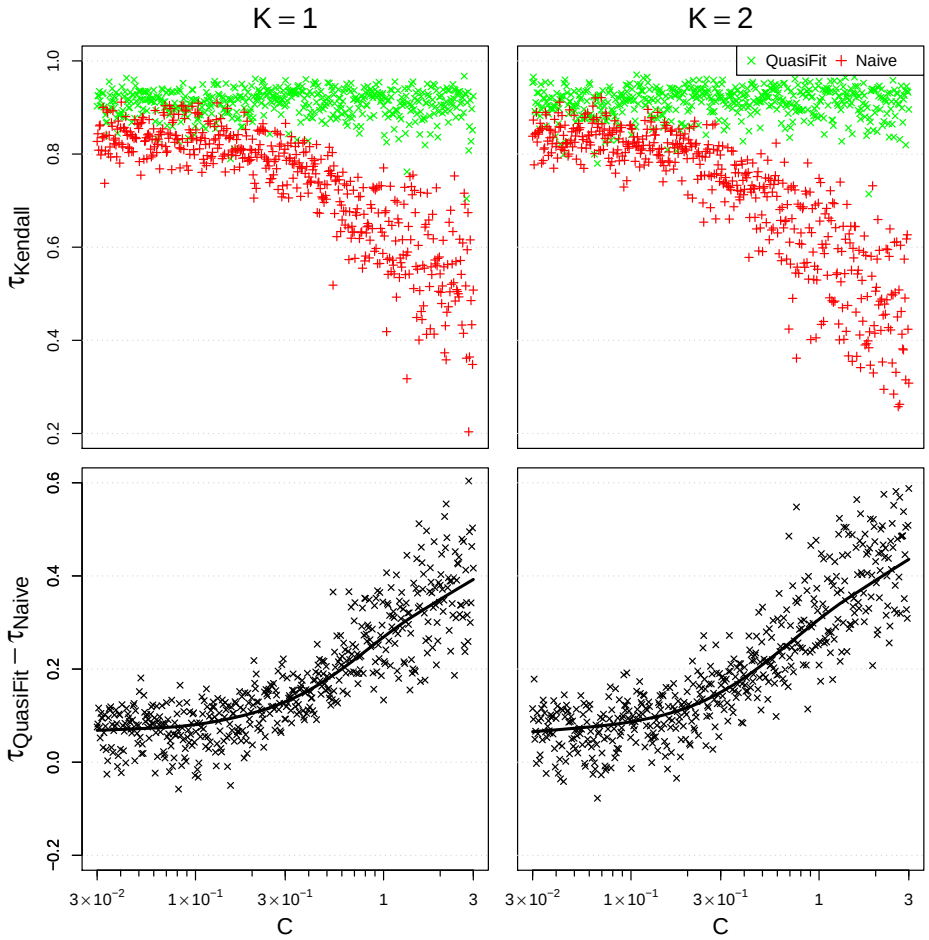

Figure S5. Accuracy of the predicted fitness landscape τ_{Kendall} as a function of the strength of epistatic relative to additive effects C. We set $L = 3$ and analyzed the cases for $K = 1, 2$. The upper row shows the ability of the two methods to recover the fitness ranks. The bottom row illustrates the differences between the two methods. The thick solid line indicates the average distance between both methods as a function of the epistatic strength C. For sake of clarity only 500 points are shown.

Notice that our estimator starts to become significantly better at recovering the ranks of the fitness landscape once epistatic effects are approximately on the order of 10% of the additive effects. This detection limit can likely be decreased with increasing coverage of the reads, as the intrinsic sampling variance of the inferred fitness estimator diminishes. Assis (2014) has shown in a study of RNA secondary structure in HIV-1 that the total epistatic contribution to the fitness landscape of a locus can make up up to 50%, which is considerably larger than our lower detection limit. In addition, da Silva *et al.* (2010) have found epistasis in HIV-1 to be important and common, where the overall epistatic contribution was orders of magnitude higher than the additive contribution in several cases.

6. Convergence diagnostics

A. Gelman and Rubin diagnostic

In order to assess whether the MCMC procedure converged to its presumed stationary distribution, we analyzed the scale reduction factor for patient 1. To this end, we ran another three independent MCMC chains beside the chain on which the results reported in the main text are based. The scale factor trajectories are plotted in Figure S6.

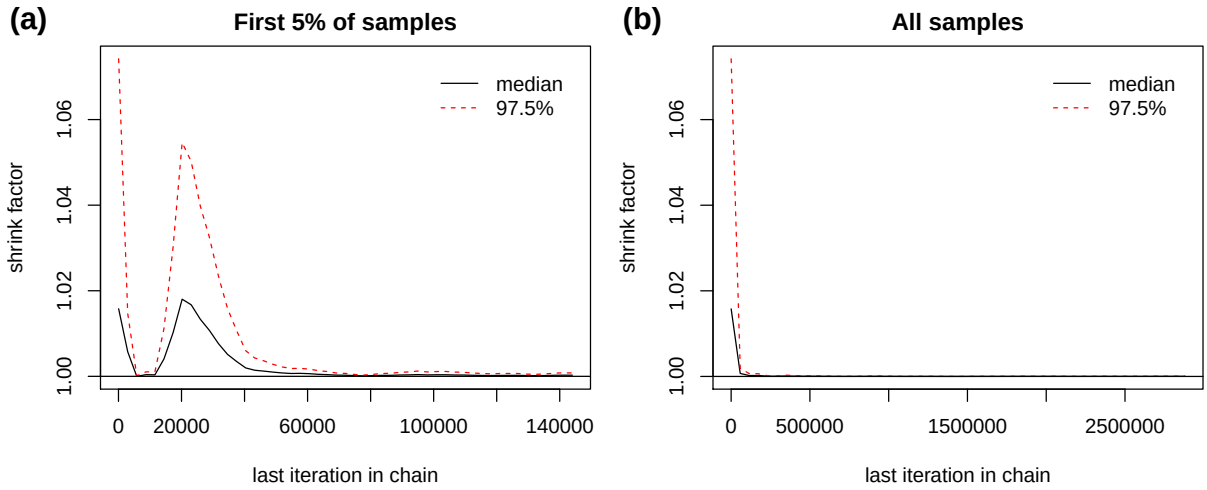

Figure S6. The Gelman-Rubin scale reduction factor. The plot in (a) shows the shrink factor vs. iteration number for the first 5% of samples. The plot in (b) shows the same shrink factor for all trial samples.

Notice how after trial count 30 000, the chains have a vanishing scale factor below 1.01, strongly suggesting convergence.

B. Autocorrelation

We determined the necessary thinning interval from autocorrelation plots (Figure S7) of one sub-chain of the MCMC procedure in the main article for patient 1.

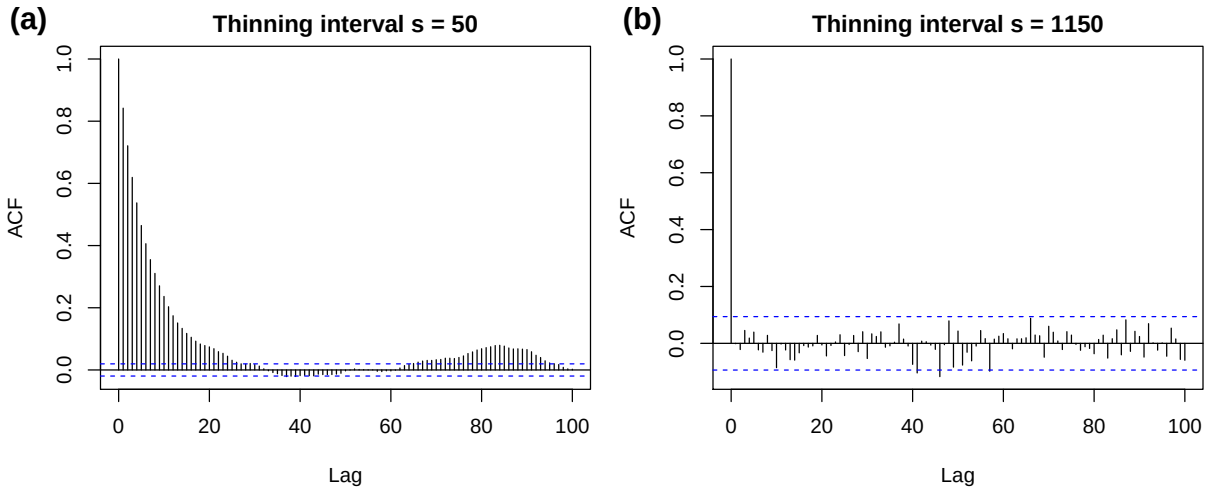

Figure S7. Autocorrelation plots for different thinning intervals. The first plot (a) indicates that even with a thinning interval of 50, significant autocorrelation remains. Plot (b) highlights that thinning interval 1150 achieves negligible autocorrelation such that samples can now be regarded as approximately independent.

At around lag 23 the autocorrelation drops below the statistical significance level. This leads to a total thinning interval of $23 \cdot 50 = 1150$ for yielding approximately independent samples from the posterior distribution.

C. Testing for differences in distributions

With thinning intervals of 1150 we proceeded to test samples from 10%–50% of trial samples with samples from 60%–100% of trial samples. Under the null hypothesis, these samples should have equal location with respect to each other if they originate from the stationary distribution. To test this null hypothesis, we employed the Wilcoxon rank sum test for all of the four independent runs in Table S3.

Table S3. Testing for differences between 40% of samples in the first half and 40% of samples in the latter half.

Runs	p-Value
1	0.3232
2	0.0751
3	0.7854
4	0.4719

None of the p-values are significant, hence we retain the null hypothesis that samples from 10%–100% originate from the same (stationary) posterior distribution.

7. Patient haplotypes

This section serves to collect the DNA sequences of haplotypes inferred from the deep sequencing data. For sake of conciseness we denote haplotypes by dropping loci with only one base and subscripting alleles at their respective loci.

Table S4. Table of haplotypes in Patient 1.

Hap. No.	Haplotype
1	$A_9A_{51}A_{74}A_{120}A_{168}A_{171}A_{183}A_{191}$
2	$A_9A_{51}A_{74}A_{120}A_{168}A_{171}A_{183}C_{191}$
3	$A_9A_{51}A_{74}A_{120}A_{168}A_{171}G_{183}A_{191}$
4	$A_9A_{51}A_{74}A_{120}A_{168}C_{171}A_{183}A_{191}$
5	$A_9A_{51}A_{74}A_{120}A_{168}C_{171}A_{183}C_{191}$
6	$A_9A_{51}A_{74}A_{120}A_{168}C_{171}G_{183}A_{191}$
7	$A_9A_{51}A_{74}A_{120}G_{168}A_{171}A_{183}A_{191}$
8	$A_9A_{51}A_{74}A_{120}G_{168}A_{171}G_{183}A_{191}$
9	$A_9A_{51}A_{74}G_{120}A_{168}A_{171}A_{183}A_{191}$
10	$A_9A_{51}A_{74}G_{120}A_{168}A_{171}A_{183}C_{191}$
11	$A_9A_{51}A_{74}G_{120}A_{168}A_{171}G_{183}A_{191}$
12	$A_9A_{51}A_{74}G_{120}A_{168}C_{171}A_{183}A_{191}$
13	$A_9A_{51}A_{74}G_{120}A_{168}C_{171}A_{183}C_{191}$
14	$A_9A_{51}A_{74}G_{120}A_{168}C_{171}G_{183}A_{191}$
15	$A_9A_{51}A_{74}G_{120}G_{168}A_{171}A_{183}A_{191}$
16	$A_9A_{51}A_{74}G_{120}G_{168}A_{171}G_{183}A_{191}$
17	$A_9A_{51}G_{74}A_{120}A_{168}A_{171}A_{183}A_{191}$
18	$A_9A_{51}G_{74}A_{120}A_{168}A_{171}A_{183}C_{191}$
19	$A_9A_{51}G_{74}A_{120}A_{168}A_{171}G_{183}A_{191}$
20	$A_9A_{51}G_{74}A_{120}A_{168}C_{171}A_{183}A_{191}$
21	$A_9A_{51}G_{74}A_{120}A_{168}C_{171}A_{183}C_{191}$
22	$A_9A_{51}G_{74}A_{120}A_{168}C_{171}G_{183}A_{191}$
23	$A_9A_{51}G_{74}A_{120}G_{168}A_{171}A_{183}A_{191}$
24	$A_9A_{51}G_{74}A_{120}G_{168}A_{171}G_{183}A_{191}$
25	$A_9A_{51}G_{74}G_{120}A_{168}A_{171}A_{183}A_{191}$
26	$A_9A_{51}G_{74}G_{120}A_{168}A_{171}A_{183}C_{191}$
27	$A_9A_{51}G_{74}G_{120}A_{168}A_{171}G_{183}A_{191}$
28	$A_9A_{51}G_{74}G_{120}A_{168}C_{171}A_{183}A_{191}$
29	$A_9A_{51}G_{74}G_{120}A_{168}C_{171}A_{183}C_{191}$
30	$A_9A_{51}G_{74}G_{120}A_{168}C_{171}G_{183}A_{191}$
31	$A_9A_{51}G_{74}G_{120}G_{168}A_{171}G_{183}A_{191}$
32	$A_9G_{51}A_{74}A_{120}A_{168}A_{171}A_{183}A_{191}$
33	$A_9G_{51}A_{74}A_{120}A_{168}A_{171}A_{183}C_{191}$
34	$A_9G_{51}A_{74}A_{120}A_{168}A_{171}G_{183}A_{191}$
35	$A_9G_{51}A_{74}A_{120}A_{168}C_{171}A_{183}A_{191}$
36	$A_9G_{51}A_{74}A_{120}A_{168}C_{171}A_{183}C_{191}$
37	$A_9G_{51}A_{74}A_{120}A_{168}C_{171}G_{183}A_{191}$
38	$A_9G_{51}A_{74}A_{120}G_{168}A_{171}A_{183}A_{191}$
39	$A_9G_{51}A_{74}A_{120}G_{168}A_{171}G_{183}A_{191}$
40	$A_9G_{51}A_{74}G_{120}A_{168}A_{171}A_{183}A_{191}$
41	$A_9G_{51}A_{74}G_{120}A_{168}A_{171}A_{183}C_{191}$
42	$A_9G_{51}A_{74}G_{120}A_{168}A_{171}G_{183}A_{191}$
43	$A_9G_{51}A_{74}G_{120}A_{168}C_{171}A_{183}A_{191}$
44	$A_9G_{51}A_{74}G_{120}A_{168}C_{171}A_{183}C_{191}$
45	$A_9G_{51}A_{74}G_{120}G_{168}A_{171}A_{183}A_{191}$
46	$A_9G_{51}A_{74}G_{120}G_{168}A_{171}G_{183}A_{191}$
47	$A_9G_{51}G_{74}A_{120}A_{168}A_{171}A_{183}A_{191}$
48	$A_9G_{51}G_{74}A_{120}A_{168}A_{171}A_{183}C_{191}$
49	$A_9G_{51}G_{74}A_{120}A_{168}A_{171}G_{183}A_{191}$
50	$A_9G_{51}G_{74}A_{120}A_{168}C_{171}A_{183}A_{191}$
51	$A_9G_{51}G_{74}A_{120}A_{168}C_{171}A_{183}C_{191}$
52	$A_9G_{51}G_{74}A_{120}A_{168}C_{171}G_{183}A_{191}$
53	$A_9G_{51}G_{74}A_{120}G_{168}A_{171}A_{183}A_{191}$
54	$A_9G_{51}G_{74}A_{120}G_{168}A_{171}G_{183}A_{191}$
55	$A_9G_{51}G_{74}G_{120}A_{168}A_{171}A_{183}A_{191}$
56	$A_9G_{51}G_{74}G_{120}A_{168}A_{171}G_{183}A_{191}$
57	$A_9G_{51}G_{74}G_{120}A_{168}C_{171}A_{183}A_{191}$
58	$A_9G_{51}G_{74}G_{120}G_{168}A_{171}G_{183}A_{191}$
59	$G_9A_{51}A_{74}A_{120}A_{168}A_{171}A_{183}A_{191}$
60	$G_9A_{51}A_{74}A_{120}A_{168}A_{171}A_{183}C_{191}$
61	$G_9A_{51}A_{74}A_{120}A_{168}A_{171}G_{183}A_{191}$
62	$G_9A_{51}A_{74}A_{120}A_{168}C_{171}A_{183}A_{191}$
63	$G_9A_{51}A_{74}A_{120}A_{168}C_{171}A_{183}C_{191}$
64	$G_9A_{51}A_{74}A_{120}A_{168}C_{171}G_{183}A_{191}$
65	$G_9A_{51}A_{74}A_{120}G_{168}A_{171}A_{183}A_{191}$
66	$G_9A_{51}A_{74}A_{120}G_{168}A_{171}G_{183}A_{191}$
67	$G_9A_{51}A_{74}G_{120}A_{168}A_{171}A_{183}A_{191}$
68	$G_9A_{51}A_{74}G_{120}A_{168}A_{171}A_{183}C_{191}$
69	$G_9A_{51}A_{74}G_{120}A_{168}C_{171}A_{183}A_{191}$
70	$G_9A_{51}A_{74}G_{120}G_{168}A_{171}G_{183}A_{191}$
71	$G_9A_{51}G_{74}A_{120}A_{168}A_{171}A_{183}A_{191}$
72	$G_9A_{51}G_{74}A_{120}A_{168}A_{171}A_{183}C_{191}$
73	$G_9A_{51}G_{74}A_{120}A_{168}A_{171}G_{183}A_{191}$
74	$G_9A_{51}G_{74}A_{120}A_{168}C_{171}A_{183}A_{191}$
75	$G_9A_{51}G_{74}A_{120}G_{168}A_{171}G_{183}A_{191}$
76	$G_9A_{51}G_{74}G_{120}A_{168}A_{171}A_{183}A_{191}$
77	$G_9A_{51}G_{74}G_{120}A_{168}C_{171}A_{183}A_{191}$
78	$G_9A_{51}G_{74}G_{120}G_{168}A_{171}G_{183}A_{191}$
79	$G_9G_{51}A_{74}A_{120}A_{168}A_{171}A_{183}A_{191}$
80	$G_9G_{51}A_{74}A_{120}A_{168}A_{171}A_{183}C_{191}$
81	$G_9G_{51}A_{74}A_{120}A_{168}C_{171}A_{183}A_{191}$
82	$G_9G_{51}A_{74}G_{120}A_{168}A_{171}A_{183}A_{191}$
83	$G_9G_{51}A_{74}G_{120}G_{168}A_{171}G_{183}A_{191}$
84	$G_9G_{51}G_{74}A_{120}A_{168}A_{171}A_{183}A_{191}$
85	$G_9G_{51}G_{74}A_{120}A_{168}C_{171}A_{183}A_{191}$
86	$G_9G_{51}G_{74}G_{120}A_{168}A_{171}A_{183}A_{191}$

The haplotypes of Patient 1 respectively Patient 2 are noted in Table S4 respectively Table S5. The graphs of the patients' fitness landscapes are shown in Figure 9 of the main article.

Table S5. Table of haplotypes in Patient 2.

Hap. No.	Haplotype
1	$A_6A_{33}A_{72}A_{74}A_{108}G_{143}G_{144}T_{192}$
2	$A_6A_{33}A_{72}A_{74}G_{108}A_{143}G_{144}T_{192}$
3	$A_6A_{33}A_{72}A_{74}G_{108}G_{143}A_{144}C_{192}$
4	$A_6A_{33}A_{72}A_{74}G_{108}G_{143}G_{144}C_{192}$
5	$A_6A_{33}A_{72}A_{74}G_{108}G_{143}G_{144}T_{192}$
6	$A_6A_{33}A_{72}G_{74}A_{108}A_{143}G_{144}G_{192}$
7	$A_6A_{33}A_{72}G_{74}A_{108}A_{143}G_{144}T_{192}$
8	$A_6A_{33}A_{72}G_{74}A_{108}G_{143}A_{144}C_{192}$
9	$A_6A_{33}A_{72}G_{74}A_{108}G_{143}A_{144}T_{192}$
10	$A_6A_{33}A_{72}G_{74}A_{108}G_{143}G_{144}C_{192}$
11	$A_6A_{33}A_{72}G_{74}A_{108}G_{143}G_{144}G_{192}$
12	$A_6A_{33}A_{72}G_{74}A_{108}G_{143}G_{144}T_{192}$
13	$A_6A_{33}A_{72}G_{74}G_{108}A_{143}A_{144}T_{192}$
14	$A_6A_{33}A_{72}G_{74}G_{108}A_{143}G_{144}C_{192}$
15	$A_6A_{33}A_{72}G_{74}G_{108}A_{143}G_{144}G_{192}$
16	$A_6A_{33}A_{72}G_{74}G_{108}A_{143}G_{144}T_{192}$
17	$A_6A_{33}A_{72}G_{74}G_{108}G_{143}A_{144}C_{192}$
18	$A_6A_{33}A_{72}G_{74}G_{108}G_{143}A_{144}G_{192}$
19	$A_6A_{33}A_{72}G_{74}G_{108}G_{143}A_{144}T_{192}$
20	$A_6A_{33}A_{72}G_{74}G_{108}G_{143}G_{144}C_{192}$
21	$A_6A_{33}A_{72}G_{74}G_{108}G_{143}G_{144}G_{192}$
22	$A_6A_{33}A_{72}G_{74}G_{108}G_{143}G_{144}T_{192}$
23	$A_6A_{33}G_{72}A_{74}G_{108}G_{143}G_{144}T_{192}$
24	$A_6A_{33}G_{72}G_{74}A_{108}G_{143}A_{144}T_{192}$
25	$A_6A_{33}G_{72}G_{74}A_{108}G_{143}G_{144}C_{192}$
26	$A_6A_{33}G_{72}G_{74}A_{108}G_{143}G_{144}T_{192}$
27	$A_6A_{33}G_{72}G_{74}G_{108}A_{143}A_{144}T_{192}$
28	$A_6A_{33}G_{72}G_{74}G_{108}A_{143}G_{144}C_{192}$
29	$A_6A_{33}G_{72}G_{74}G_{108}A_{143}G_{144}G_{192}$
30	$A_6A_{33}G_{72}G_{74}G_{108}A_{143}G_{144}T_{192}$
31	$A_6A_{33}G_{72}G_{74}G_{108}G_{143}A_{144}T_{192}$
32	$A_6A_{33}G_{72}G_{74}G_{108}G_{143}G_{144}C_{192}$
33	$A_6A_{33}G_{72}G_{74}G_{108}G_{143}G_{144}G_{192}$
34	$A_6A_{33}G_{72}G_{74}G_{108}G_{143}G_{144}T_{192}$
35	$A_6G_{33}A_{72}A_{74}G_{108}G_{143}G_{144}G_{192}$
36	$A_6G_{33}A_{72}A_{74}G_{108}G_{143}G_{144}T_{192}$
37	$A_6G_{33}A_{72}G_{74}A_{108}G_{143}G_{144}T_{192}$
38	$A_6G_{33}A_{72}G_{74}G_{108}A_{143}G_{144}C_{192}$
39	$A_6G_{33}A_{72}G_{74}G_{108}A_{143}G_{144}G_{192}$
40	$A_6G_{33}A_{72}G_{74}G_{108}G_{143}A_{144}G_{192}$
41	$A_6G_{33}A_{72}G_{74}G_{108}G_{143}A_{144}T_{192}$
42	$A_6G_{33}A_{72}G_{74}G_{108}G_{143}G_{144}C_{192}$
43	$A_6G_{33}A_{72}G_{74}G_{108}G_{143}G_{144}G_{192}$
44	$A_6G_{33}A_{72}G_{74}G_{108}G_{143}G_{144}T_{192}$
45	$A_6G_{33}G_{72}G_{74}A_{108}G_{143}G_{144}T_{192}$
46	$A_6G_{33}G_{72}G_{74}G_{108}G_{143}G_{144}G_{192}$
47	$A_6G_{33}G_{72}G_{74}G_{108}G_{143}G_{144}T_{192}$
48	$G_6A_{33}A_{72}A_{74}A_{108}A_{143}G_{144}T_{192}$
49	$G_6A_{33}A_{72}A_{74}A_{108}G_{143}A_{144}T_{192}$
50	$G_6A_{33}A_{72}A_{74}A_{108}G_{143}G_{144}C_{192}$
51	$G_6A_{33}A_{72}A_{74}A_{108}G_{143}G_{144}G_{192}$
52	$G_6A_{33}A_{72}A_{74}A_{108}G_{143}G_{144}T_{192}$
53	$G_6A_{33}A_{72}A_{74}G_{108}A_{143}A_{144}T_{192}$
54	$G_6A_{33}A_{72}A_{74}G_{108}A_{143}G_{144}T_{192}$
55	$G_6A_{33}A_{72}A_{74}G_{108}G_{143}A_{144}T_{192}$
56	$G_6A_{33}A_{72}A_{74}G_{108}G_{143}G_{144}C_{192}$
57	$G_6A_{33}A_{72}A_{74}G_{108}G_{143}G_{144}G_{192}$
58	$G_6A_{33}A_{72}A_{74}G_{108}G_{143}G_{144}T_{192}$
59	$G_6A_{33}A_{72}G_{74}A_{108}A_{143}A_{144}C_{192}$
60	$G_6A_{33}A_{72}G_{74}A_{108}A_{143}A_{144}T_{192}$
61	$G_6A_{33}A_{72}G_{74}A_{108}A_{143}G_{144}C_{192}$
62	$G_6A_{33}A_{72}G_{74}A_{108}A_{143}G_{144}G_{192}$
63	$G_6A_{33}A_{72}G_{74}A_{108}A_{143}G_{144}T_{192}$
64	$G_6A_{33}A_{72}G_{74}A_{108}G_{143}A_{144}C_{192}$
65	$G_6A_{33}A_{72}G_{74}A_{108}G_{143}A_{144}G_{192}$
66	$G_6A_{33}A_{72}G_{74}A_{108}G_{143}A_{144}T_{192}$
67	$G_6A_{33}A_{72}G_{74}A_{108}G_{143}G_{144}C_{192}$
68	$G_6A_{33}A_{72}G_{74}A_{108}G_{143}G_{144}G_{192}$
69	$G_6A_{33}A_{72}G_{74}A_{108}G_{143}G_{144}T_{192}$
70	$G_6A_{33}A_{72}G_{74}G_{108}A_{143}A_{144}C_{192}$
71	$G_6A_{33}A_{72}G_{74}G_{108}A_{143}A_{144}G_{192}$
72	$G_6A_{33}A_{72}G_{74}G_{108}A_{143}A_{144}T_{192}$
73	$G_6A_{33}A_{72}G_{74}G_{108}A_{143}G_{144}C_{192}$
74	$G_6A_{33}A_{72}G_{74}G_{108}A_{143}G_{144}G_{192}$
75	$G_6A_{33}A_{72}G_{74}G_{108}A_{143}G_{144}T_{192}$
76	$G_6A_{33}A_{72}G_{74}G_{108}G_{143}A_{144}C_{192}$
77	$G_6A_{33}A_{72}G_{74}G_{108}G_{143}A_{144}G_{192}$
78	$G_6A_{33}A_{72}G_{74}G_{108}G_{143}A_{144}T_{192}$
79	$G_6A_{33}A_{72}G_{74}G_{108}G_{143}G_{144}C_{192}$
80	$G_6A_{33}A_{72}G_{74}G_{108}G_{143}G_{144}G_{192}$
81	$G_6A_{33}A_{72}G_{74}G_{108}G_{143}G_{144}T_{192}$
82	$G_6A_{33}G_{72}A_{74}A_{108}G_{143}G_{144}T_{192}$
83	$G_6A_{33}G_{72}A_{74}G_{108}G_{143}G_{144}C_{192}$
84	$G_6A_{33}G_{72}A_{74}G_{108}G_{143}G_{144}T_{192}$
85	$G_6A_{33}G_{72}G_{74}A_{108}A_{143}G_{144}T_{192}$
86	$G_6A_{33}G_{72}G_{74}A_{108}G_{143}A_{144}G_{192}$
87	$G_6A_{33}G_{72}G_{74}A_{108}G_{143}A_{144}T_{192}$
88	$G_6A_{33}G_{72}G_{74}A_{108}G_{143}G_{144}C_{192}$
89	$G_6A_{33}G_{72}G_{74}A_{108}G_{143}G_{144}G_{192}$
90	$G_6A_{33}G_{72}G_{74}A_{108}G_{143}G_{144}T_{192}$
91	$G_6A_{33}G_{72}G_{74}G_{108}A_{143}A_{144}T_{192}$
92	$G_6A_{33}G_{72}G_{74}G_{108}A_{143}G_{144}C_{192}$
93	$G_6A_{33}G_{72}G_{74}G_{108}A_{143}G_{144}T_{192}$
94	$G_6A_{33}G_{72}G_{74}G_{108}G_{143}A_{144}C_{192}$
95	$G_6A_{33}G_{72}G_{74}G_{108}G_{143}A_{144}G_{192}$
96	$G_6A_{33}G_{72}G_{74}G_{108}G_{143}A_{144}T_{192}$
97	$G_6A_{33}G_{72}G_{74}G_{108}G_{143}G_{144}C_{192}$
98	$G_6A_{33}G_{72}G_{74}G_{108}G_{143}G_{144}G_{192}$
99	$G_6A_{33}G_{72}G_{74}G_{108}G_{143}G_{144}T_{192}$
100	$G_6G_{33}A_{72}A_{74}G_{108}G_{143}G_{144}T_{192}$
101	$G_6G_{33}A_{72}G_{74}A_{108}A_{143}G_{144}T_{192}$
102	$G_6G_{33}A_{72}G_{74}A_{108}G_{143}A_{144}C_{192}$
103	$G_6G_{33}A_{72}G_{74}A_{108}G_{143}A_{144}T_{192}$
104	$G_6G_{33}A_{72}G_{74}A_{108}G_{143}G_{144}C_{192}$
105	$G_6G_{33}A_{72}G_{74}A_{108}G_{143}G_{144}T_{192}$
106	$G_6G_{33}A_{72}G_{74}G_{108}A_{143}A_{144}C_{192}$
107	$G_6G_{33}A_{72}G_{74}G_{108}A_{143}A_{144}T_{192}$
108	$G_6G_{33}A_{72}G_{74}G_{108}A_{143}G_{144}C_{192}$
109	$G_6G_{33}A_{72}G_{74}G_{108}A_{143}G_{144}G_{192}$
110	$G_6G_{33}A_{72}G_{74}G_{108}A_{143}G_{144}T_{192}$
111	$G_6G_{33}A_{72}G_{74}G_{108}G_{143}A_{144}G_{192}$
112	$G_6G_{33}A_{72}G_{74}G_{108}G_{143}A_{144}T_{192}$
113	$G_6G_{33}A_{72}G_{74}G_{108}G_{143}G_{144}C_{192}$
114	$G_6G_{33}A_{72}G_{74}G_{108}G_{143}G_{144}G_{192}$
115	$G_6G_{33}A_{72}G_{74}G_{108}G_{143}G_{144}T_{192}$
116	$G_6G_{33}G_{72}G_{74}A_{108}G_{143}G_{144}C_{192}$
117	$G_6G_{33}G_{72}G_{74}A_{108}G_{143}G_{144}T_{192}$
118	$G_6G_{33}G_{72}G_{74}G_{108}A_{143}G_{144}T_{192}$
119	$G_6G_{33}G_{72}G_{74}G_{108}G_{143}A_{144}C_{192}$
120	$G_6G_{33}G_{72}G_{74}G_{108}G_{143}A_{144}T_{192}$
121	$G_6G_{33}G_{72}G_{74}G_{108}G_{143}G_{144}C_{192}$
122	$G_6G_{33}G_{72}G_{74}G_{108}G_{143}G_{144}G_{192}$
123	$G_6G_{33}G_{72}G_{74}G_{108}G_{143}G_{144}T_{192}$

8. Codon usage effects

In the main article in section *Fitness landscapes of clinical p7 quasispecies* we analyzed the bi-allelic two loci peptide space for illustration purposes and as a proof-of-concept of our developed method. Here we show the results of looking at fitness differences of codons at synonymous loci. To this end, we iterated over all amino acid residues and analyzed those positions where heterogeneity exists in DNA sequences but not in the translated peptides. In order to analyze codon usage effects, we marginalized out the effects of all other loci, by defining equivalence classes for the synonymous codons, similar to the approach used for defining equivalence classes for peptides in section *Fitness landscapes of clinical p7 quasispecies* of the main article. We have analyzed synonymous codons for patient 1 and patient 2 and have summarized the results in Table S6 respectively Table S7.

Table S6. Codon usage in patient 1. The wild-type is indicated by the letters **wt** and defined as the major allele, whereas the mutant allele is (**mt**) defined to be the minor allele. The variable $\bar{p}$ denotes the posterior average frequency of the respective codon.

Amino acid position	**Amino acid**	**wt**		**mt**	
		Codon	$\bar{p}_{\text{wt}}$	Codon	$\bar{p}_{\text{mt}}$
3	Ala	GCA	85.5%	GCG	14.5%
17	Arg	AGA	87.8%	AGG	12.2%
40	Arg	AGA	92.1%	AGG	7.9%
56	Glu	GAA	82.5%	GAG	17.5%
57	Gly	GGA	74.6%	GGC	25.4%
61	Lys	AAA	80.0%	AAG	20.0%

Table S7. Codon usage in patient 2. The wild-type is indicated by the letters **wt** and defined as the major allele, whereas the mutant allele ($\mathbf{mt}_{1,2}$) is defined to be the first and (if applicable) second minor allele. The variable $\bar{p}$ denotes the posterior average frequency of the respective codon. Notice the tri-allelic locus at amino acid position 64.

Amino acid position	**Amino acid**	**wt**		$\mathbf{mt}_1$		$\mathbf{mt}_2$	
		Codon	$\bar{p}_{\text{wt}}$	Codon	$\bar{p}_{\text{mt}_1}$	Codon	$\bar{p}_{\text{mt}_2}$
2	Glu	GAG	88.4%	GAA	11.6%		
11	Ala	GCA	94.5%	GCG	5.5%		
24	Arg	AGA	91.9%	AGG	8.1%		
36	Gly	GGG	87.8%	GGA	12.2%		
64	Thr	ACT	88.4%	ACC	8.5%	ACG	3.1%

All codons could be credibly inferred to differ in their fitness, with the wild-type codon fitter than average and all mutant codons less fit than average. Given the large frequencies of the wild-type alleles, this is not unexpected. Codon usage is a known cause for fitness differences *in vivo* (Ermolaeva *et al.*, 2001).

9. Runtime evaluation

In order to better understand when the asymptotic complexity of $\mathcal{O}(n^3)$ is reached, we ran our sampler on artificial data. To this end, we reduced the alphabet to a binary set $\mathcal{A} = \{\text{A, G}\}$ and set the length of the genomic space under study to $L = \{1, \ldots, 9\}$, such that the total number of haplotypes will be $n = 2^L$. All simulations were performed with $N_{\text{trials}} = 100$ per chain and a total of 512 chains, thus having simulated a total of 51 200 MCMC trials. For each simulation, we recorded the time required for simulating the MCMC trials, divided the total runtime by 51 200 in order to yield the average runtime per MCMC trial. All simulations were conducted on an Intel Xeon E5-2697 CPU with one simulation thread. In order to estimate the transition to the asymptotic regime, we estimate two models of runtime

$$t(n) = a + b \cdot n + c \cdot n^2 + d \cdot n^3 \tag{9.1}$$

and the asymptotic model

$$t(n) = d \cdot n^3 \tag{9.2}$$

The full model (9.1) was fitted by employing non-linear least squares (NLS) on the log-transformed data, while the latter (9.2) was fitted by performing NLS on just the last three log-transformed data points. The fitted models are depicted in Figure S8 and confirm that beyond $n \approx 64$ the asymptotic regime is practically reached. In this regime the calculation of the matrix determinant in (4.13) is the rate-determining step, whereas below this limit non-cubic memory allocation and function overhead contribute a sizable portion to the computational runtime.

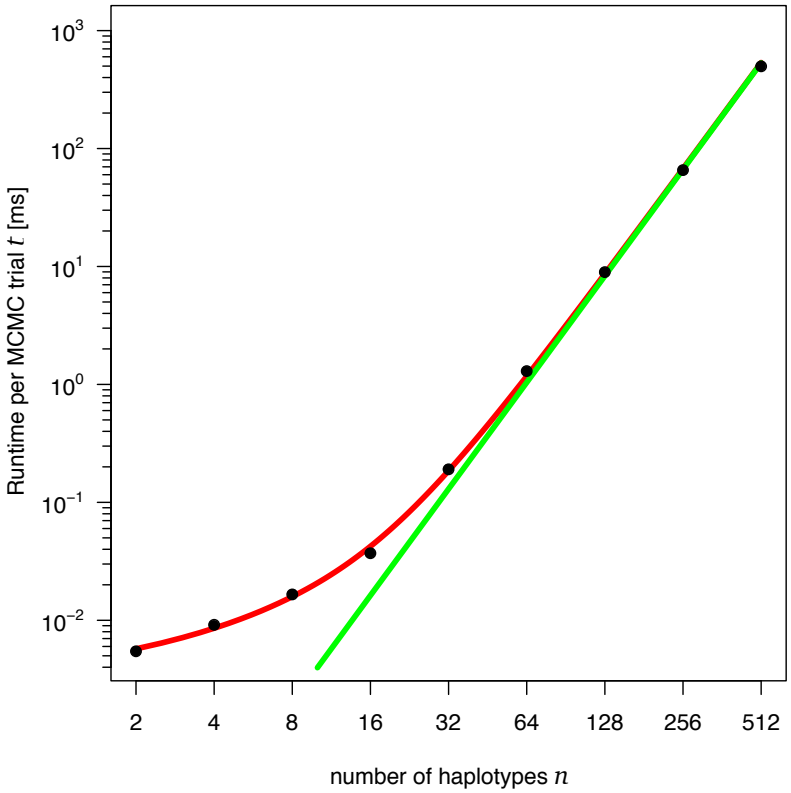

Figure S8. Graph of the per MCMC trial runtime t versus the number of haplotypes n. The red curve represents the best fit of (9.1) whereas the green model represents the asymptotic complexity (9.2).

References

Abram, M. E., Ferris, A. L., Shao, W., Alvord, W. G., and Hughes, S. H. (2010). Nature, position, and frequency of mutations made in a single cycle of HIV-1 replication. *Journal of Virology*, **84**(19), 9864–9878.

Aitchison, J. (1982). The Statistical Analysis of Compositional Data. *Journal of the Royal Statistical Society. Series B (Methodological)*, **44**(2), 139–177.

Assis, R. (2014). Strong Epistatic Selection on the RNA Secondary Structure of HIV. *PLOS Pathogens*, **10**(9), e1004363.

Bapat, R. B. and Raghavan, T. E. S. (1997). *Nonnegative matrices and applications*, volume 64. Cambridge University Press.

da Silva, J., Coetzer, M., Nedellec, R., Pastore, C., and Mosier, D. E. (2010). Fitness Epistasis and Constraints on Adaptation in a Human Immunodeficiency Virus Type 1 Protein Region. *Genetics*, **185**(1), 293–303.

Ermolaeva, M. D. *et al.* (2001). Synonymous codon usage in bacteria. *Current Issues in Molecular Biology*, **3**(4), 91–97.

Kimura, M. (1980). A simple method for estimating evolutionary rates of base substitutions through comparative studies of nucleotide sequences. *Journal of Molecular Evolution*, **16**(2), 111–120.

Searle, S. (1982). *Matrix Algebra Useful for Statistics*. Wiley-Interscience.